Thermal Conductivity of Moist Cellular Concrete—Experimental and Numerical Study

Dariusz J. Gawin, D.Sc. **Jan Kosny, Ph.D.** **Kenneth Wilkes, Ph.D.**
Member ASHRAE

ABSTRACT

Hygrothermal phenomena in cellular concrete samples during the steady-state tests of thermal conductivity have been numerically simulated. It has been found that the most important factor for the accuracy of these tests is the initial moisture content of the test specimens. In the range of 70-85% RH the "heat pipe" mechanism is of importance, causing an additional latent heat transport, which increases apparent thermal conductivity. This phenomenon is strongly influenced by the material porosity and inner structure of pores, i.e., the shape of the sorption isotherms. Outside this range of relative humidity, errors caused by moisture transport and related heat effects are negligible. The error caused by moisture has been found for the cellular concrete with density of 600 kg/m^3 to be smaller than for the 400 kg/m^3 one. For smaller values of specimen thickness, the error is smaller. The smaller the temperature difference used between plates of the heat-flow-meter apparatus, the smaller is the moisture induced error observed. On the basis of the computer simulation results, graphs and tables with correction factors are developed to improve the accuracy of steady-state measurements of thermal conductivity for cellular concrete.

Some experimental results of steady-state measurements of thermal conductivity by use of the heat-flow-meter apparatus are presented. They concern three types of cellular concrete with densities of 400, 500, or 600 kg/m^3 and additionally for two types of lightweight concrete, i.e., wood-concrete and EPS-concrete, at various moisture contents. These results qualitatively confirm the theoretical predictions presented in the first part of the paper.

INTRODUCTION

The aim of this study is evaluation of moisture influence on the thermal conductivity of various types of cellular concrete. In particular, we are interested in estimation of the accuracy for thermal conductivity measurements of these materials, commonly done by use of a heat-flow-meter apparatus based on the steady-state hot plate method. When moist materials are being tested in such an apparatus, thermo-diffusion changes the moisture space distribution and causes additional convective and latent heat transport. These phenomena are believed to be a source of considerable test errors, hence, unsteady heat flow methods are often used for moist materials. These methods are usually based on the various shape "impulse" changes such as "Dirac's delta" or the ramp Heaviside's functions of temperature of a heat source placed in a tested material. The thermal parameters of the material (thermal diffusivity and sometimes thermal capacity) are determined by comparison of measured temperature history characteristics to the corresponding analytical solutions of the problem. In practice, it is very difficult to maintain conditions such as contact thermal resistances, keeping the shape of the temperature impulse strictly the same as in the theoretical problem. Hence, in these methods test errors are large and often difficult to evaluate reliably.

In this study, we have theoretically analyzed the steady-state hot plate measurements for moist cellular concrete with density of 400 or 600 kg/m^3 by use of computer simulation based on a nonlinear mathematical model of hygrothermal phenomena in porous building materials. The HMTRA model of coupled heat and moisture transfer in capillary-porous

Dariusz J. Gawin is associate professor in the Department of Building Physics and Building Materials at the Technical University of Lodz, Poland. **Jan Kosny** and **Kenneth Wilkes** are senior researchers at the Oak Ridge National Laboratory, Oak Ridge, Tenn.

materials developed by Gawin et al. (1995, 1996) has been used. It takes into account all important energy and mass transport phenomena, separately for each phase of the medium, phase changes (evaporation, condensation, adsorption, desorption), and hygrothermal deformations of the material.

This analysis allowed us to better understand the physical phenomena causing apparent increase of thermal conductivity during these tests and to evaluate errors caused by moisture migration. The effect of factors such as specimen thickness, plate temperature difference, and initial moisture content on the accuracy of the steady-state thermal conductivity tests has been analyzed.

Finally, the thermal conductivity of three types of cellular concrete and two other types of lightweight concrete, wood-concrete and EPS-concrete, in dry and several moist states, has been experimentally tested by use of the heat-flow-meter apparatus to verify our theoretical predictions.

NUMERICAL MODEL OF COUPLED HYGROTHERMAL PHENOMENA IN BUILDING MATERIALS

The mathematical model used for analyzing the hygrothermal behavior of cellular concrete was originally derived by Gawin et al. (1995). Salient features of the model and the numerical solution technique can be found in Gawin et al. (1995, 1996). In this model porous building materials are treated as a multiphase system, which are locally in thermodynamic equilibrium. The voids of the skeleton are filled partly with liquid water and partly with a gas phase. The liquid phase consists of bound water, which is present in the whole range of moisture content, and capillary water, which appears when water content exceeds the upper limit of the hygroscopic region. The gas phase is a mixture of dry air and water vapor that is assumed to behave as an ideal gas. The chosen primary variables of the model are: gas pressure p_g, capillary pressure p_c, temperature T, and the displacement vector of the solid matrix $\mathbf{u}$.

The model consists of five balance equations. The mass balance of the dry air includes both Fickian (diffusive) and Darcian (advectional) flows:

$$\phi\frac{\partial}{\partial t}[(1-S)\rho_{ga}] + \alpha(1-S)\rho_{ga}\frac{\partial}{\partial t}(\nabla\cdot\mathbf{u}) + \nabla\cdot(\rho_{ga}\boldsymbol{v}_g) - \nabla\cdot(\rho_g\boldsymbol{v}^d_{gw}) = 0 \tag{1}$$

The symbols used in this and the next equations are explained in the nomenclature section at the end of this paper. The subscripts s, ga, gw, and g are related to solid, dry air, water vapor, and gas phase, respectively.

The mass balances of liquid water and of vapor, summed together to eliminate the source term related to phase changes, form the mass balance equation for the water species,

$$\phi\frac{\partial}{\partial t}[(1-S)\rho_{gw}] + \alpha(1-S)\rho_{gw}\frac{\partial}{\partial t}(\nabla\cdot\mathbf{u}) + \nabla\cdot(\rho_{gw}\boldsymbol{v}_g) + \nabla\cdot(\rho_g\boldsymbol{v}^d_{gw}) = -\phi\rho_w\frac{\partial S}{\partial t} - \alpha S\rho_w\frac{\partial}{\partial t}(\nabla\cdot\mathbf{u}) + \nabla\cdot(\rho_w\boldsymbol{v}_w) \tag{2}$$

where the subscript w is related to liquid water.

The enthalpy balance equation of the whole medium includes the heat effects of the phase-change process, as well as the convective and latent heat transfer,

$$(\rho C_p)_{eff}\frac{\partial T}{\partial t} + [C_{pw}\rho_w\boldsymbol{v}_w + C_{pg}\rho_{gw}\boldsymbol{v}_g]\cdot\nabla T - \nabla\cdot(\lambda_{eff}\nabla T) = \Delta h_{vap}\left[\phi\rho_w\frac{\partial S}{\partial t} + \alpha S\rho_w\frac{\partial}{\partial t}(\nabla\cdot\mathbf{u}) - \nabla\cdot(\rho_w\boldsymbol{v}_w)\right]. \tag{3}$$

Introducing Bishop's effective stress tensor σ" (Schrefler and Gawin 1996), which causes the deformations of a concrete, the linear momentum balance equation of the whole medium is given by

$$div(\sigma'' - \alpha p\mathbf{I}) + [(1-\phi)\rho_s + \phi S\rho_w + \phi(1-S)\rho_g]\boldsymbol{g} = \mathbf{0}. \tag{4}$$

where $p = p_g - S p_c$ is average pressure of the fluids (water and air) contained in pores of the material, $\mathbf{I}$ the unit, second order tensor, and $\mathbf{g}$ the acceleration of gravity.

The time derivative of porosity has been eliminated from Equations 1-3 by summing the mass conservation equations for the dry air, water vapor, and capillary water or adsorbed water with the mass conservation equation of the solid phase,

$$\frac{\partial}{\partial t}[(1-\phi)\rho_s] + \nabla\cdot[(1-\phi)\rho_s\boldsymbol{v}_s] = 0. \tag{5}$$

The balance Equations (1-4) are completed by an appropriate set of constitutive and state equations, some thermodynamic relationships, as well as initial and boundary conditions (Gawin et al. 1995; Gawin and Schrefler 1996; Gawin 2000). The latter ones allow defining both the fixed (e.g., equal to zero at impermeable or adiabatic boundaries) and convective heat and mass fluxes, as well as radiative heat fluxes (e.g., solar radiation) on the external surfaces of the building structures being analyzed. The model takes into account temperature, capillary pressure, and gas pressure dependence of material properties, thermal conductivity and capacity, intrinsic and relative permeability, effective vapor diffusivity, Young's modulus, and Poisson's ratio, as well as sorption isotherm models. The same concerns physical properties of water and vapor, i.e., specific latent heat of evaporation and adsorption, water and gas viscosity, and water vapor diffusivity in air.

Discretization in space of the governing equations is carried out by means of the finite element method. The unknown variables are expressed in terms of their nodal values as

$$p_g = p_g(t) = \boldsymbol{N}_p\bar{\boldsymbol{p}}_g(t), \qquad p_c = p_c(t) = \boldsymbol{N}_p\bar{\boldsymbol{p}}_c(t),$$
$$T = T(t) = \boldsymbol{N}_t\bar{\boldsymbol{T}}(t), \qquad u = u(t) = \boldsymbol{N}_u\bar{\boldsymbol{u}}(t)\,. \tag{6}$$

The integral or weak form of the heat and mass transfer equations, after introduction of the constitutive equations, was obtained by means of a generalized Galerkin's type procedure (weighted residuals) (Zienkiewicz and Taylor 1989) and can be expressed in matrix form as (Gawin et al. 1995; Gawin and Schrefler 1996; Gawin 2000)

$$\mathbf{C}(\mathbf{x})\frac{\partial x}{\partial t} + \mathbf{K}(\mathbf{x})\mathbf{x} + \mathbf{f}(\mathbf{x}) = 0 \tag{7}$$

where $\mathbf{x}^T = \{\bar{\boldsymbol{p}}_g, \bar{\boldsymbol{p}}_c, \bar{\boldsymbol{T}}, \bar{\boldsymbol{u}}\}$ and $\mathbf{C}(\mathbf{x})$, $\mathbf{K}(\mathbf{x})$, $\mathbf{f}(\mathbf{x})$ are nonlinear (matrix) coefficients.

The time discretization is accomplished by means of a fully implicit finite difference scheme (backward difference) (Zienkiewicz and Taylor 1989),

$$\mathbf{C}_{n+1}\frac{\mathbf{x}_{n+1} - \mathbf{x}_n}{\Delta t} + \mathbf{K}_{n+1}\mathbf{x}_{n+1} + \mathbf{f}_{n+1} = 0\,, \tag{8}$$

where $\mathbf{C}_{n+1} = \mathbf{C}(\mathbf{x}_{n+1})$, $\mathbf{B}_{n+1} = \mathbf{B}(\mathbf{x}_{n+1})$, $\mathbf{f}_{n+1} = \mathbf{f}(\mathbf{x}_{n+1})$, n is the time step index, and Δt the length of the time step.

Because of the nonlinearity of Equation 8 the solution is obtained with a Newton-Raphson type procedure (Zienkiewicz and Taylor 1989),

$$\begin{aligned}
&\frac{1}{\Delta t}\left[\frac{\partial \mathbf{C}^l_{n+1}}{\partial \mathbf{x}}(\mathbf{x}^l_{n+1} - \mathbf{x}_n) + \mathbf{C}^l_{n+1}\right]\Delta\mathbf{x}^l_{n+1} \\
&+\left[\frac{\partial \mathbf{K}^l_{n+1}}{\partial \mathbf{x}}\mathbf{x}^l_{n+1} + \mathbf{K}^l_{n+1} + \frac{\partial \mathbf{f}^l_{n+1}}{\partial \mathbf{x}}\right]\Delta\mathbf{x}^l_{n+1} \\
&= -\left[\mathbf{C}^l_{n+1}\frac{\mathbf{x}^l_{n+1} - \mathbf{x}_n}{\Delta t} + \mathbf{K}^l_{n+1}\mathbf{x}_{n+1} + \mathbf{f}^l_{n+1}\right]
\end{aligned} \tag{9}$$

where l is the iteration index, and at the end of each iteration the primary variables are updated as follows:

$$\mathbf{x}^{l+1}_{n+1} = \mathbf{x}^l_{n+1} + \Delta\mathbf{x}^l_{n+1}\,. \tag{10}$$

A special "switching" procedure (Gawin and Schrefler 1996), which deals with fully and partially saturated media present at the same time in the different parts of the domain, is applied. Based on the presented discretization, the HMTRA-DEF research computer code was developed for the solution of the nonlinear and nonsymmetrical system of equations governing heat and mass transfer in deforming porous media. It has already been successfully applied for solution of several problems concerning hygrothermal phenomena in building materials and soils (Gawin et al. 1995; Gawin and Schrefler 1996; Gawin 2000).

COMPUTER SIMULATION OF HYGROTHERMAL PHENOMENA IN CELLULAR CONCRETE DURING A STEADY-STATE HOT PLATE THERMAL CONDUCTIVITY TEST

Hygrothermal behavior of cellular concrete samples during steady-state hot plate thermal conductivity tests has been simulated by use of the computer model described above. Two different types of autoclaved aerated concrete (AAC), with densities of 400 or 600 kg/m^3, have been analyzed. The main material parameters of these materials, assumed in our computations, are shown in Table 1. Four different values of the specimen thickness have been analyzed: d = 2.5, 5.0, 7.5, and 10 cm. The sample has been discretized by use of 26 (26 × 1) eight-node finite elements of variable size (smaller ones near the surfaces). Different specimen thicknesses have been obtained by "scaling" the dimensions of the individual elements. The first 24 hours of the hygrothermal transient, after beginning the hot plate measurement, have been simulated. At various stages of computations, different time step lengths have been used ranging from 1 s at the beginning up to 150 s at the advanced stages. Cellular concrete specimens have been assumed to be initially in thermodynamic equilibrium with the ambient air at 295.15 K with relative humidity corresponding to the case analyzed: φ = 40%, 50%, 60%, 70%, 80%, 85%, 90%, and 95%. During the tests done with the heat-flow-meter apparatus, temperature on the surfaces of the cellular concrete specimens reached the prescribed value after 4-5 minutes. Then it was maintained within range ±0.01 K. Hence, in our simulations, the constant temperature values on the

Table 1. Material Properties for AACs Used in Computer Simulations

Material property	Units	AAC 400	AAC 600
Dry state apparent density, ρ_o	kg/m^3	400	600
Porosity, Φ	-	0.81	0.70
Thermal conductivity of dry material, λ_{dry}	W/(m·K)	0.115	0.162
Specific heat of dry material, C_{dry}	J/(kg·K)	850	850
Intrinsic permeability, K_o	m^2	$2.5\cdot10^{-17}$	$2\cdot10^{-17}$
Young's modulus, E	GPa	1.5	2.3
Poison's ratio, ν	-	0.25	0.25

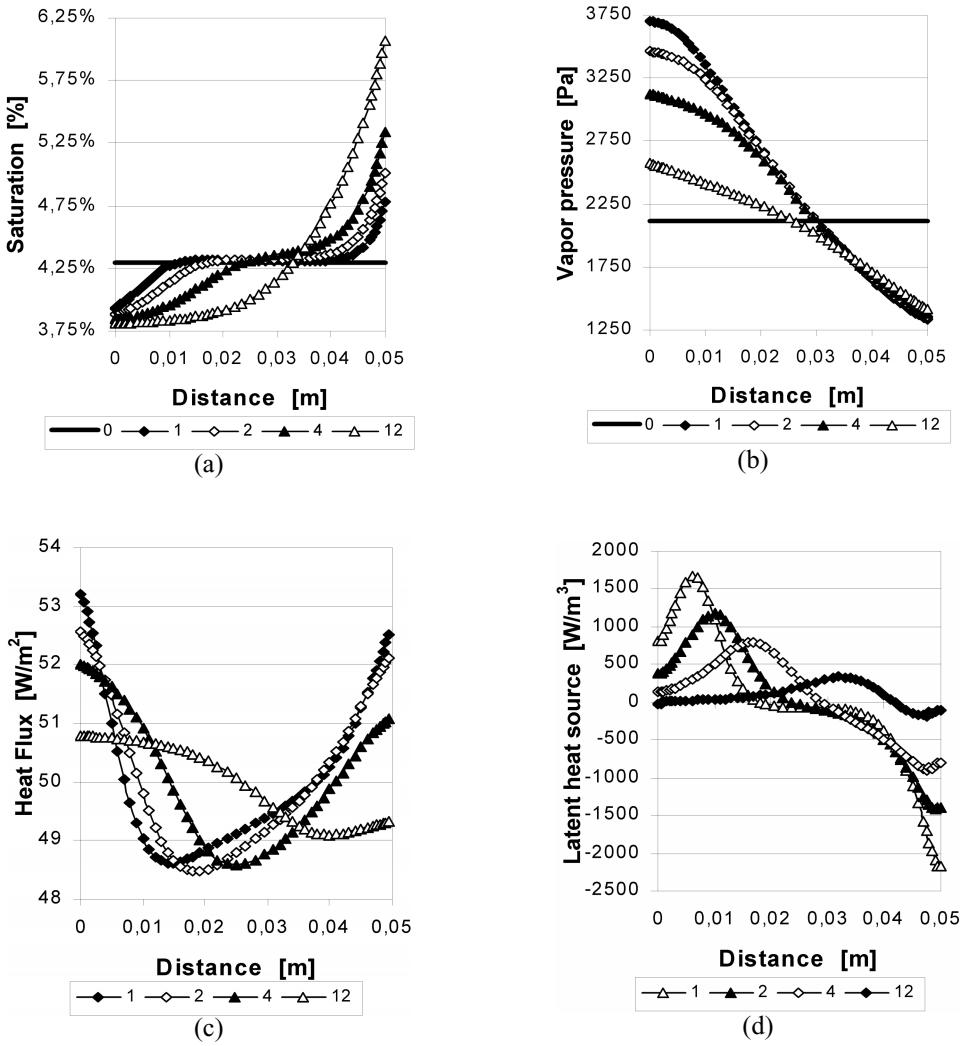

Figure 1 *The distribution of (a) saturation degree, (b) vapor pressure, (c) conductive heat flux, and (d) heat sources related to phase changes, at different time stations (time in hours), during the steady-state thermal conductivity test of AAC 400 with the initial relative humidity* φ *= 80% RH, d = 5.0 cm, and* ΔT *= 20 K (x = 0 corresponds to the hot plate).*

heated and cooled surfaces of the specimen, T_{heat} (for $x = 0$) and T_{cool} (for $x = D$, where D is the specimen thickness), have been assumed as the boundary conditions for heat exchange. Three temperature differences between the specimen surfaces, $\Delta T = T_{heat} - T_{cool}$, ΔT = 6, 10, and 20 K, with the same "average" value of 297.15 K, have been considered. Impermeable boundaries, for water and vapor, for the specimen have been assumed for moisture exchange.

The effect of several factors, such as the specimen thickness, the temperature difference across the specimen, the initial moisture content of the material, and the measurement time, upon accuracy of the steady-state thermal conductivity test (i.e., ratio of the measured and the "real" values, corresponding to homogenous moisture distribution) have been analyzed. These results allow better understanding of the physical phenomena causing an apparent increase of thermal conductivity and an evaluation of errors caused by migration and redistribution of moisture during the test. A brief summary and discussion of the results of our simulations are presented below.

Physical Phenomena in a Moist AAC Specimen During the Test

During the steady-state hot plate thermal conductivity test, a specimen of moist cellular concrete is exposed to a temperature gradient. This causes moisture migration (sometimes called thermo-diffusion) and its redistribution (Figure 1a), as well as changes of vapor pressure (Figure 1b). The

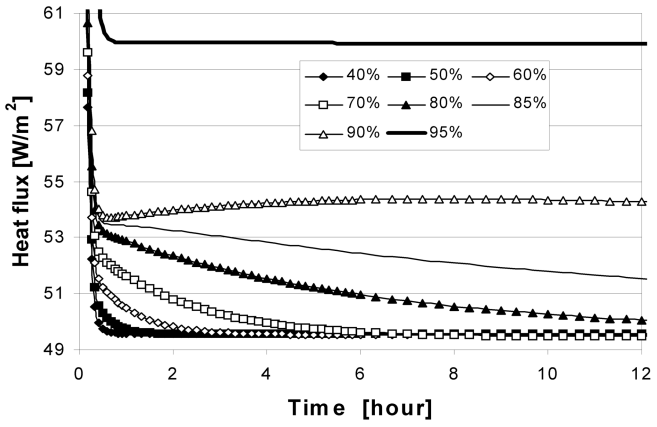

Figure 2 *Time histories of the average heat flux during the steady-state thermal conductivity test of the AAC 400 samples (d = 5.0 cm and ΔT = 20 K) with different values of the initial moisture content (the relative humidities corresponding to these values are used as the lines description).*

cooled and heated surfaces of the specimen are impermeable both for water and gas; hence, the total mass of moisture contained within the sample is constant (neglecting some imperfections in contact between the sample surfaces and the apparatus plates and, related to them, possible transversal mass flow during real tests). One observes a circulation of moisture inside the material pores: vapor flows toward the cooling plate (opposite to the pressure gradient direction, Figure 2b) and liquid water flows in the opposite direction, toward the lower moisture content, Figure 1a. Water evaporates near the heating plate and the vapor condenses near the cooling plate (Figure 1c) resulting in a considerable latent heat transport. All these physical phenomena constitute the well-known "heat pipe" mechanism. Due to moisture redistribution, phase changes, and latent heat transport, the heat flux during the test is variable in space and time, Figure 1c and Figure 2, and not constant as assumed in the steady-state methods. This causes test error.

One of the criteria used in a heat-flow-meter apparatus for evaluation of steady state is constant in time, within an assumed range, value of the average heat flux. The measured heat fluxes on the heating and cooling plates should be approximately equal to one another. The results of our simulations show that for the moist cellular concrete specimens, in equilibrium with the air relative humidity approximately between 70% and 85%, these fluxes change for a period of time, Figure 2, that is longer than normally necessary for a test of the dry material. Then, for the material with relative humidity exceeding 90%, the difference of heat fluxes on the specimen surfaces can be greater than 7% of their average value, Figure 3. Because of these phenomena some special settings, different from the normal ones, must be used when testing the moist specimens of cellular concrete.

During the steady-state hot plate tests, the measured thermal conductivity, λ, is determined from:

$$\lambda = \frac{d_{aver}(q_{heat} + q_{cool})}{2 \cdot (T_{heat} - T_{cool})} \tag{11}$$

where T and q are temperatures and heat fluxes measured at the heating and cooling surfaces (denoted with subscripts "*heat*" and "*cool*," respectively), and d_{aver} is the average thickness of the specimen, usually determined at the beginning of a test.

Modern heat-flow-meter apparatuses maintain constant temperatures of the plates within the range ±0.01K, and the sample thickness does not change significantly during the test (omitting its very small changes related to thermal dilatation and hygral deformations—shrinkage and swelling); hence, exact values of the heat fluxes are crucial for the test accuracy. When these fluxes are changing gradually due to moisture migration and redistribution during the test, Figure 2, the measured value of thermal conductivity is variable, as well. This may be a source of considerable test errors.

There are three reasons for the test errors: a change of moisture distribution in the sample, convective transport of heat by the flowing fluids, and, finally, an additional heat flux caused by latent heat transfer due to a "heat pipe" mechanism. The error caused by the first phenomenon (an apparent decrease of the measured thermal conductivity) in the analyzed materials with φ ≤ 95% after 24 hours never exceeded 0.7% for the ACC 400 and 0.3% for the ACC 600. Approximately, it increased proportionally to the test duration as our analysis showed based on the simulation results concerning the saturation degree (moisture content). Thus, one can expect that for a typical test duration of three to six hours, for the highest considered initial moisture content, corresponding to the relative humidity φ = 95%, this error will be four to eight times smaller and has no practical importance.

During the steady-state thermal conductivity tests of moist materials, we observe a small flow of liquid water within the pores, Figure 1a, and related to this convective heat flow. The gas phase (moist air) remains practically stagnant if one neglects some very small gas flows caused by gas pressure gradients due to initial temperature changes. The resultant convective heat flow caused by the diffusion of the dry air and vapor particles is negligible (they move in opposite directions and have similar specific heats), when compared to effects of the liquid water convection. For the temperature difference ΔT = 20 K, the convective heat flow in liquid water may be estimated to be about 30 times smaller than the latent heat flow in vapor (assuming the specific heat of water $c_w \cong 4.18$ kJ/(kg·K) and the heat of water evaporation $\Delta h_{vap} \cong 2.5$ MJ/kg), if the corresponding mass fluxes are assumed to be equal to one another. The results of our simulations showed that in the moist cellular concretes the liquid water fluxes were slightly higher than the vapor fluxes because the moisture content near the cooling plate gradually increased with time, Figure 1a. But even for the worst of the analyzed cases, i.e., ΔT = 20K, d =

Table 2. Values of k-Ratio for AAC-400 Specimen with Thickness of 5.0 cm and Different Values of Measurement Time, Temperature Difference, and Initial Relative Humidity

Measurement Time [h]	ΔT [K]	φ =70%	φ = 80%	φ = 85%	φ = 90%	φ = 95%
2	6	1.029	1.049	1.046	1.021	1.000
	10	1.028	1.049	1.048	1.024	1.001
	20	1.022	1.046	1.054	1.037	1.004
4	6	1.015	1.040	1.041	1.021	1.001
	10	1.013	1.038	1.043	1.025	1.002
	20	1.006	1.031	1.046	1.041	1.004
6	6	1.007	1.032	1.037	1.020	1.001
	10	1.005	1.029	1.039	1.025	1.002
	20	0.999	1.020	1.038	1.043	1.004

2.5 cm, and φ = 95%, the water flux after 24 hours was only about 50% higher than the vapor flux; thus, the latent heat flow was about 20 times greater than the convective heat flow related to the liquid water migration. This explicitly shows that the latter one is negligible in comparison to the latent heat transport, which has the most important influence on the accuracy of the steady-state thermal conductivity tests of moist cellular concretes. To evaluate the effect of this phenomenon on the test accuracy, we have calculated *k*, the ratio of the "measured" thermal conductivity, i.e., calculated from Equation 11 for the actual values of temperatures and heat fluxes on the sample surfaces, obtained from our computer simulations, and the "real" one (i.e., for the initial, homogenous moisture distribution corresponding to the analyzed value of air relative humidity). The *k*-ratio characterizes only an error induced by moisture migration and related latent heat transport, assuming that all necessary physical quantities are measured without any test error. Exemplary time histories of the *k*-ratio for the AAC 400 kg/m^3 and AAC 600 kg/m^3 samples with a thickness of 5.0 cm and ΔT = 20 K, for different values of the initial relative humidity of the materials, are presented in Figure 4. As can be seen, the moisture-induced apparent increase of thermal conductivity was the highest for RH between 70% and 85%, reaching values up to 5.7% for the first material and 1.2% for the second one. These considerable differences in the error values show that the analyzed phenomena are strongly influenced by the material density (porosity) and other physical properties related to inner structure of pores, e.g., a shape of the sorption isotherms, intrinsic permeability. Outside this relative humidity range, errors caused by moisture movement are much smaller.

Effect of the Temperature Difference of the Heating and Cooling Plates

The results presented above show that the temperature gradients in moist AAC samples cause latent heat flow to be a source of test errors. An obvious method to reduce these gradients is decreasing the temperature difference, ΔT, between the heating and cooling plates during the steady-state thermal conductivity tests. To analyze the effect of this quantity on the moisture-induced test error, the values of *k*-ratio were calculated (see Table 1) for the results of simulations of the AAC 400 sample (in this material the effect of the latent heat flow is more distinct) with thickness of 5.0 cm for three different values of ΔT. As can be seen in Table 3, the effect of the temperature difference depends on the initial moisture content of the specimen and the time when the measurement was done. For relative humidity values smaller than about 80%, application of a lower temperature difference did not improve the test accuracy, but this improvement is visible for relative humidity higher than 85%. Hence, for φ ≤ 80% one should use the higher temperature difference ΔT and longer time Δt_{init} before starting the measurements. On the contrary, for φ ≥ 85% the values of ΔT and Δt_{init} should be as small as possible, but taking into account other requirements of the test (e.g., the duration of thermal transient).

Effect of the Specimen Thickness

Another method for decreasing the temperature gradient during a steady-state thermal conductivity test is to use a thicker specimen. To analyze this possibility, the values of the *k*-ratio were calculated for the AAC 400 samples with thicknesses of 2.5, 5.0, 7.5, and 10 cm for different times of measurement as shown in Table 3. In analysis of these results, one should take into account that the thicker the analyzed specimen, the longer the time of thermal transient before the measurements could be started. However, it is clearly visible that increasing the specimen thickness does not have a positive influence on the test accuracy when the initial relative humidity is φ ≤ 85%. This can be explained by a decreasing effect of "moisture redistribution" (see "Physical Phenomena in a moist AAC Specimen During the Test"), causing for the thicker samples a smaller apparent decrease of the measured thermal conductivity, which compensates in part for the effect of latent heat transport. For φ ≥ 90% the "heat pipe" mechanism becomes less important, see Figure 2, while the moisture redistribution effect is more pronounced.

Table 3. Values of k-Ratio for AAC 400 Sample with Temperature Difference ΔT=20K and for Different Values of Specimen Thickness, Measurement Time, and Initial Relative Humidity

Measurement Time [h]	Thickness [cm]	φ =70%	φ = 80%	φ = 85%	φ = 90%	φ = 95%
2	2.5	0.997	1.012	1.032	1.044	1.004
	5.0	1.022	1.046	1.054	1.037	1.004
	7.5	1.038	1.057	1.057	1.031	1.002
	10.0	1.046	1.060	1.056	1.028	1.003
4	2.5	0.995	0.997	1.013	1.038	1.003
	5.0	1.006	1.031	1.046	1.041	1.004
	7.5	1.025	1.049	1.055	1.036	1.004
	10.0	1.039	1.057	1.057	1.032	1.003
6	2.5	0.995	0.994	1.004	1.030	1.003
	5.0	0.999	1.018	1.037	1.044	1.004
	7.5	1.013	1.039	1.051	1.039	1.004
	10.0	1.027	1.050	1.055	1.035	1.004
12	2.5	0.995	0.994	0.998	1.016	1.002
	5.0	0.995	1.001	1.020	1.042	1.004
	7.5	1.000	1.021	1.040	1.043	1.004
	10.0	1.010	1.037	1.049	1.039	1.004

Table 4. Maximal Values of Initial Relative Humidity of AAC 400 Samples of Different Thickness (for ΔT=20K) to Maintain Moisture-Induced Test Error ε_{moist} within the Fixed Limits

Error ε_{moist}	d = 2.5 cm (1 in.)			d = 5.0 cm (2 in.)		
	t = 2h	t = 4h	t = 6h	t = 2h	t = 4h	t = 6h
1%	79%	84%	86%	63%	72%	76%
2%	82%	86%	88%	68%	76%	80%
3%	84%	88%	90%	73%	79%	83%
4%	87%			77%	83%	86%
5%				81%		
Error ε_{moist}	**d = 7.5 cm (3 in.)**			**d = 10.0 cm (4 in.)**		
	t = 2h	t = 4h	t = 2h	t = 4h	t = 2h	t = 4h
1%	55%	62%	67%	48%	55%	60%
2%	60%	67%	72%	55%	61%	65%
3%	65%	72%	76%	60%	66%	70%
4%	70%	76%	76%	65%	70%	74%
5%	75%	80%	83%	71%	76%	79%
6%				78%	83%	84%

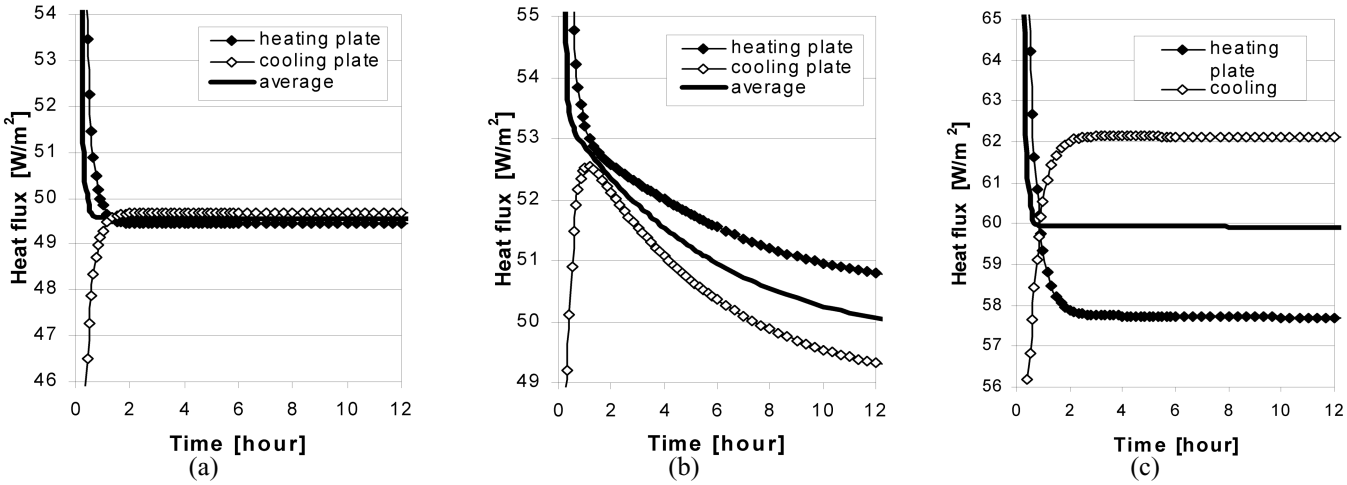

Figure 3 *Time histories of the heat fluxes during the steady-state thermal conductivity tests of the AAC 400 samples (d = 5.0 cm and ΔT = 20K) for different values of the initial moisture content, corresponding to the air relative humidities: (a) φ = 40%, (b) φ = 80%, (c) φ = 95%.*

Table 5. Thermal Conductivity of Various Types of Lightweight Concrete as a Linear Function of Mass Moisture Content

Material	λ_{dry} [W/(m·K)]	*K* [W/(m·K)]	R^2
AAC 400 kg/m^3	0.114	0.0065	0.951
AAC 500 kg/m^3	0.141	0.0067	0.999
AAC 600 kg/m^3	0.165	0.0057	0.962
Wood concrete	0.147	0.0033	0.985
EPS concrete	0.109	0.0023	0.972

On the basis of the present analysis, several graphs and tables with correcting factors were developed to evaluate and improve the accuracy of the steady-state measurements of thermal conductivity for AACs; see, for example, Table 4.

RESULTS OF STEADY-STATE THERMAL CONDUCTIVITY TESTS

Thermal conductivity data for three different types of autoclaved aerated concrete (ACC) blocks with densities of 400, 500, or 600 kg/m^3 and for two types of lightweight concrete, i.e., wood-concrete and EPS-concrete, with various hygroscopic moisture contents, were measured in ORNL Material Properties Laboratory following ASTM C518 procedure. The highest analyzed moisture content was about 14.2% by weight (wt.%) and it was reached after two months of moisture sorption. Following the results of analysis presented above in "Computer Simulation of Hyrothermal Phenomena in Cellular Concrete During a Steady-State Hot Plate Thermal Conductivity Test," the temperature difference between the plates $\Delta T \cong 8$ K and the specimens with thickness of about 5.0 cm were used. Before the test, they were kept in an environment with a specified relative humidity for at least one month and then sealed and kept in the laboratory for at least three days to obtain more homogenous moisture distribution.

The results of the tests are presented in Figure 5. As could be expected, thermal conductivity of these moist materials is considerably higher compared to the oven dry state. The strongest influence of the mass moisture content on thermal conductivity was observed for AAC with density of 400 kg/m^3 and 500 kg/m^3 and the lowest one for EPS-concrete. It has been found that an increase of thermal conductivity for the analyzed materials in the hygroscopic moisture range is proportional to the mass moisture content. It can be approximated, with accuracy sufficient for most practical applications, using a linear relationship. The parameters λ_{dry} [W/(m·K)] and *K* [W/(m·K)] of the approximated linear relationship $\lambda = \lambda_{dry} + K \cdot u$, expressing thermal conductivity λ of the moist materials as a function of the mass moisture content *u* [kg/kg], and their correlation coefficients R^2 are presented in Table 5.

The results of the tests done for the moist AACs confirmed, at least quantitatively, the results of the theoretical analysis presented above in "Computer Simulation of Hyrothermal Phenomena in Cellular Concrete During a Steady-State Hot Plate Thermal Conductivity Test." Figure 6 shows the changes in time of the heat fluxes measured in the samples of AAC 400 with moisture content $u = 0$ wt.% (oven dry, $\Delta T = 8.0$ K) and $u = 2.1$ wt.% ($\varphi \cong 75\%$, $\Delta T = 7.8$ K). As can be

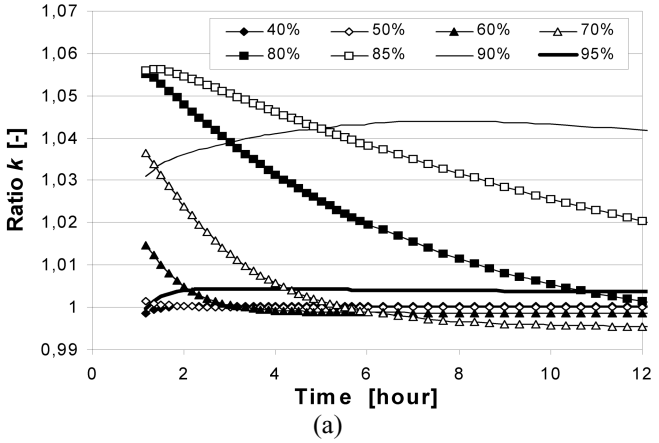

(a)

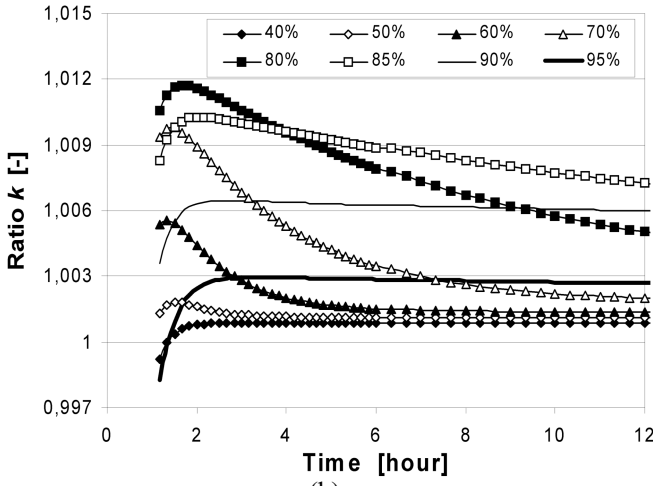

(b)

Figure 4 *Time histories of the* k*-ratio during the steady-state thermal conductivity tests of the AAC samples with different values of the initial relative humidity (*d *= 5.0 cm and* ΔT *= 20 K) for two different material densities: (a) 400 kg/m^3; (b) 600 kg/m^3.*

seen, for the dry sample the measured heat flux was practically constant, while for the moist one it gradually decreased, as predicted by our simulations, see Figure 3.

During the tests of the moist specimens, the temperature differences, ΔT, were slightly different for various moisture contents. They were also different from the values used in our simulations. Hence, a direct comparison of the heat fluxes was impossible. For this reason we calculated the ratios between the actual values of thermal conductivity and the base ones (i.e., determined two hours after beginning of the tests) to compare their change in time for different levels of moisture content. The results for the AAC 400 with different moisture content are shown in Figure 7. These can be qualitatively compared to the values of the *k*-ratio calculated for $\Delta T = 20$ K in "Physical Phenomena in a Moist AAC Specimen During the

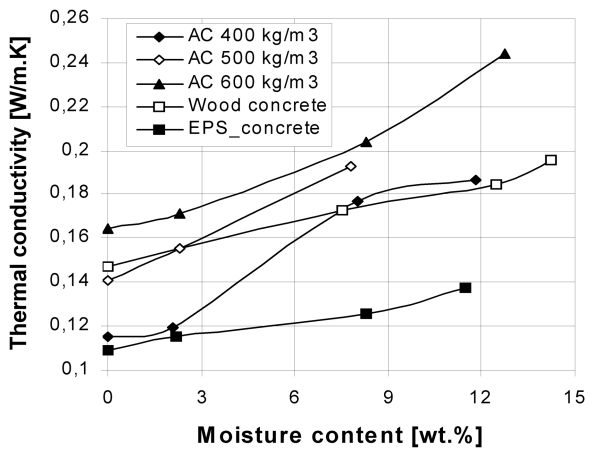

Figure 5 *Results of the steady-state measurements of the thermal conductivity for various types of lightweight concrete with different moisture content.*

Test," Figure 4. The change in time of the measured thermal conductivity for the higher moisture content, u = 8.0 wt.%, was slower (or at least similar) compared to the case with u = 2.1 wt.%. This was also predicted by our simulations, Figure 4.

CONCLUSIONS

The results of the theoretical computations and some experimental measurements show that a steady-state method can be used for measurements of thermal conductivity for moist cellular concrete in hygroscopic moisture range, where the effect of gravity on moisture distribution is negligible. Heat flux changes caused by moisture movement and latent heat transfer are of the greatest importance for moisture contents corresponding to the relative humidities in the range between 70% and 85%. But even in this range they are small enough to perform the steady-state test and obtain reasonable results for practical applications. The error caused by moisture is about three to four times smaller for AAC 600 kg/m^3 than for 400 kg/m^3 one. For smaller values of specimen thickness, the error is smaller. For relative humidities between 70% and 85%, the smaller the temperature difference between plates of the apparatus that is used, the smaller is the moisture-induced error observed. For higher relative humidity values, the error depends to a lesser extent on this temperature difference and the sample thickness.

NOMENCLATURE

C_p = isobaric specific heat
p_c = capillary pressure, $p_c = p_g - p_w$
p_g = gas pressure
p_w = water pressure
S = degree of pore saturation with liquid water
T = temperature
t = time

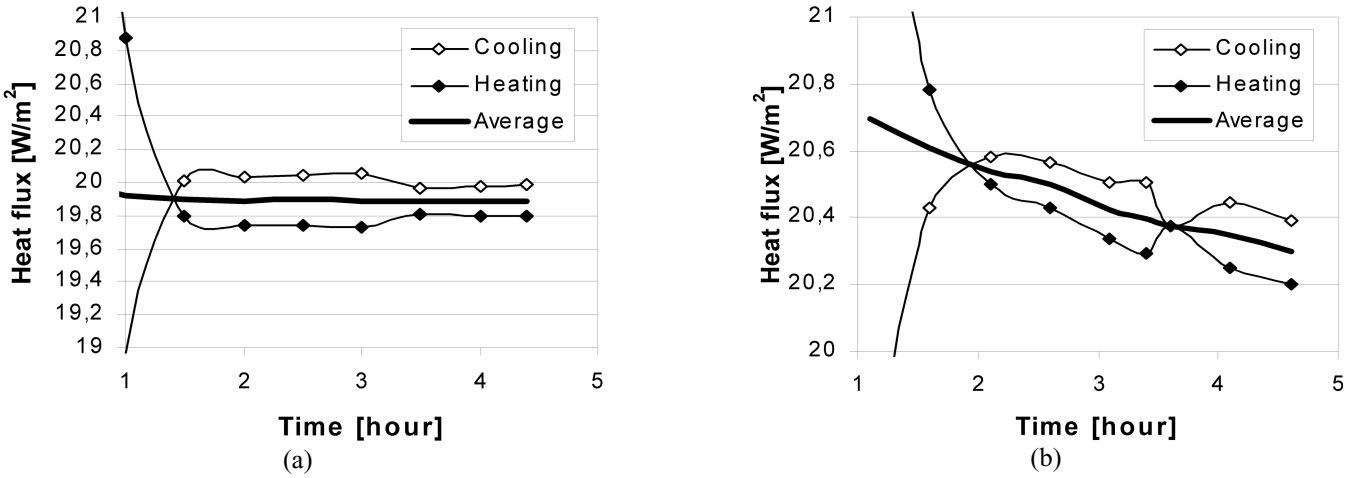

Figure 6 *Change in time of the measured heat fluxes in the sample of the AAC 400 kg/m3 for two different values of moisture content: (a) 0 wt.%; (b) 2.1 wt.% (φ ≅ 75%).*

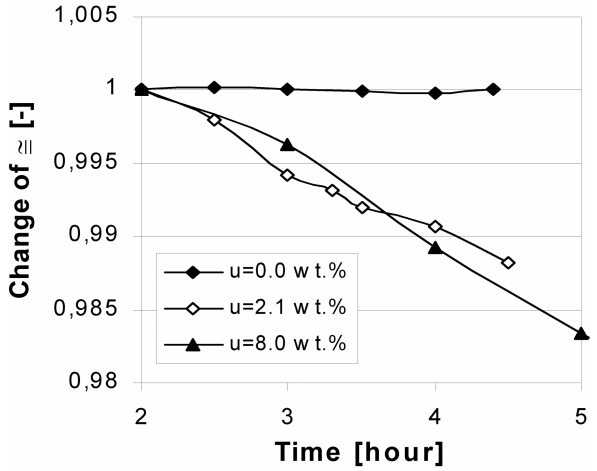

Figure 7 *Change in time of the ratio between the thermal conductivity values measured at various time stations and the base value (for 2 hours) in sample of AAC 400 kg/m3 (ΔT ≅ 8 K) for three different values of moisture content: u = 0 wt.% (oven dry), u = 2.1 wt.% (φ ≅ 75% RH), and u = 8.0 wt.% (φ ≅ 85% RH).*

u = displacement vector of the solid matrix (the material skeleton)

$\boldsymbol{v}$ = velocity relative to the solid skeleton

$\boldsymbol{v}^{d}$ = relative average diffusion velocity

α = Biot's constant

Δh_{vap} = specific enthalpy of the phase change

ϕ = porosity

λ_{eff} = effective thermal conductivity

ρ = density

$(\rho C_p)_{eff}$ = the effective thermal capacity

REFERENCES

Gawin, D., P. Baggio, and B.A. Schrefler. 1995. Coupled heat, water and gas flow in deformable porous media. *Int. J. Num. Meth. in Fluids*, vol. 20: 969-987.

Gawin, D., and B.A. Schrefler. 1996. Thermo- hydro-mechanical analysis of partially saturated porous materials. *Engineering Computations* 13 (7): 113-143.

Schrefler, B.A., and D. Gawin, D. 1996. The effective stress principle: incremental or finite form? *Int. J. Num. Anal. Meth. in Geomechanics* 20(11): 785-815.

Gawin, D. 2000. *Modelling of Coupled Hygro-thermal Phenomena in Building Materials and Building Components* (in Polish), pp. 303. Scientific Bulletin of Łódź Technical University, No 853, Editions of Łódź Technical University, ISSN 0137-4834, Łódź.

Zienkiewicz, O.C., and R.L. Taylor. 1989. *The Finite Element Method*, Vol. 1, 4th ed. London: Mc Graw Hill.